SHARK-NIR, toward the end of the construction phase

Jacopo Farinato*[a,i], Maria Bergomi[a,i], Andrea Bianco[b], Federico Biondi[a,i], Elena Carolo[a,i], Alexis Carlotti[c], Simonetta Chinellato[a,i], Marco De Pascale[a], Marco Dima[a,i], Valentina D'Orazi[a], Davide Greggio[a,i], Philip Hinz[d], Luigi Lessio[a,i], Luca Marafatto[a,i], Dino Mesa[a], Lars Mohr[e], Manny Montoya[d], Gabriele Umbriaco[a,h,i], Daniele Vassallo[a,i], Valentina Viotto[a,i], Alessio Zanutta[b], Simone Antoniucci[f,i], Carmelo Arcidiacono[a,i], Francesca Bacciotti[g], Carlo Baffa[g], Andrea Baruffolo[a], Angela Bongiorno[f], Laird Close[f], Simone Di Filippo[a,h,i], Simone Esposito[g,i], Giancarlo Farisato[a,i], Olivier Guyon[f], Demetrio Magrin[a,i], Fernando Pedichini[f,i], Enrico Pinna[g,i], Elisa Portaluri[a,i], Alfio Puglisi[g,i], Kalyan Kumar Radhakrishnan Santhakumari[a,i], Roberto Ragazzoni[a,i], Fabio Rossi[g,i], Marco Stangalini[f,i]

[a]INAF Padova, Vicolo dell'osservatorio 5, 35122, Padova, Italy;
[b]INAF Brera, Via Brera, 28, 20121 Milano MI
[c]Institut de Planétologie et d'Astrophysique de Grenoble, 414, Rue de la Piscine, Domaine Universitaire, 38400 St-Martin d'Hères (France);
[d]University of Arizona, Department of Astronomy/Steward Observatory, 933 North Cherry Avenue, Tucson, AZ, USA;
[e]Max Planck Institute for Astronomy, Königstuhl 17, 69117 Heidelberg, Germany;
[f]INAF Roma, Via di Frascati 33, 00040 Monte Porzio Catone, Italy;
[g]INAF Arcetri, Largo Enrico Fermi, 5, 50125 Firenze, Italy;
[h]Università di Padova, Dipartimento di Fisica e Astronomia, Vicolo dell'Osservatorio 3, 35122, Padova, Italy;
[i]ADONI, Laboratorio Nazionale di Ottica Adattiva Italiano

ABSTRACT

Both Sharks (NIR and VIS) are undergoing the construction phase, and they are getting close to the moment in which they will be installed at the Large Binocular Telescope, one for each arm. They are conceived to make binocular coronagraphic observations, trying to catch planets also in close synergy with LBTI, used in coronagraphic fashion too. SHARK-NIR operates in Y-J-H bands and together with SHARK-VIS, covering the visible bandwidth, and LMIRCam, operating from K to M bands, will allow simultaneous observations from V to M band. The upgrade of the LBT AO systems to SOUL will push the extreme strehl regime to fainter magnitude, opening to science not fully covered with similar instruments, both in the number of targets to be studied looking for planets and for other very interesting science topics: jets and disks targets will increase quite a lot and AGN and QSO may become an interesting extragalactic topic to be studied due to the increased AO performance in the faint end regime.

SHARK-NIR can operate in direct imaging, coronagraphic imaging, dual band coronagraphic imaging and low resolution spectroscopic mode. A number of coronagraphic techniques have been studied for possible implementation, and Gaussian Lyot, Shaped Pupil and Four Quadrant have been initially selected for implementation, even if there is room to upgrade to other techniques. The instrument has a couple of peculiar features, such as a fast internal TT loop to minimize the residual jitter and a local NCPA correction, performed through a DM inside the instrument itself. We report here about the SHARK-NIR status, which is in the AIV phase, that should finish by the end of the year, bringing in this way the first photons to the instrument in 2020.

Keywords: planet finding, coronagraphy, pyramid sensor, adaptive secondary, extreme adaptive optics, large binocular telescope

1. INTRODUCTION

SHARK (System for coronagraphy with High order Adaptive optics from R to K band) [1] is an instrument proposed for the LBT[2] in the framework of the "2014 Call for Proposals for Instrument Upgrades and New Instruments". It is composed by two channels: SHARK-VIS[3], working from 0.5µm to 1µm, and SHARK-NIR[4], working in the near infrared bands, Y, J and H, operating from 0.96µm to 1.7µm. SHARK-NIR is currently in the AIV phase, to be soon installed at LBT. The science achievable with SHARK will range from exoplanet search and characterization to star forming regions, where jets and disks will be explored in their innermost regions.
The resolution achievable with a 10-m class telescope allows to access, in the NIR domain, gaseous giant planets of Jupiter size or bigger, which still is a very challenging task to be achieved, due to the very high contrast and vicinity to the hosting star required. There are several scientific goals to be possibly exploited in the exo-planet science case, ranging from the direct detection of unknown giant planets, to the follow up of known planets (through spectroscopic and photometric characterization).They require of course the implementation of a spectroscopic mode with modest

spectral resolution that is currently foreseen in SHARK-NIR through a long slit positioned into the intermediate focal plane.

But the science to be exploited with SHARK-NIR is definitely not only limited to the exo-planets case. In fact, the study of proto-planetary disks is fundamental to comprehend the formation of our own solar system as well as of extrasolar planetary systems. To understand how matter aggregates to form the building blocks of planetary bodies, there is the need to investigate not only the evolution of the disk itself, but also the role of jets in shaping its structure. This requires observing the system at high angular resolution as close as possible to the parent star, occulting its light to enhance the area where the interplay between the accretion and ejection of matter dominates the dynamics.

Other very interesting and challenging topics can be found in the extragalactic science, where the capabilities of SHARK-NIR in terms of spatial resolution and contrast enhancement may be applied to study the AGN-host relations as well as Dumped Ly-α systems (DLAs), to constrain the Black Hole feeding mechanism and to trace, in bright quasars, molecular outflows powerful enough to clean the inner kilo-parsec and quench the star formation.

Furthermore, there is important feature of the LBT AO which will give to SHARK-NIR the possibility to exploit unique coronagraphic science. The Pyramid WFS has a demonstrated gain in sensitivity compared to other WFSs commonly used, such as the Shack-Hartmann ([10], [11], [12], [13], [14]). This fact gives to the LBT AO systems the capability to achieve high SR (of the order of 70%) at moderately faint magnitude (R~12 or even occasionally fainter, depending on the observing conditions).

Such an excellent performance will be further enhanced with the implementation of the AO upgrade SOUL (**S**ingle Conjugated Adaptive **O**ptics **U**pgrade for **L**BT), giving the capability to achieve SRs as high as 70% at magnitudes >13 (REF).

This performance will open the field of high-contrast AO coronagraphic imaging to stars much fainter than required by other coronagraphic instruments, allowing deep search for planets around targets like, e.g., M dwarfs in nearby young associations and solar type stars in nearby star-forming regions (Taurus-Auriga at 140 pc). Also in the extragalactic field, the sample of AGN and, above all, of Quasars to be explored will go from a few tenths to a few hundreds, changing the perspective of the science to be achieved. This is definitely the characteristic that may give to SHARK-NIR unique opportunities in the coronagraphic instrument scenario.

The spectral coverage of the two SHARKS in coronagraphic direct imaging mode, used in combination with LMIRcam of LBTI[8], will go from R to M band, giving to LBT the unique capability to make contemporary coronagraphic observations with three instruments:

- SHARK-NIR on one arm, operating between Y and H bands
- SHARK-VIS and LMIRcam on the other arm, that will operate contemporary (through a dedicated dichroic splitting the visible from the infrared light), the first in V,R I and Z bands, the second in K, L and M bands which is a unique scenario for coronagraphy in the framework of the modern planet finders.

SHARK-NIR is currently in the AIV phase, and in this paper we describe the activities ongoing to complete the integration of the instrument in mid-2020, to have it possibly installed at the telescope by the end of next year.

2. SHARK DESCRIPTION

SHARK will be installed at the entrance foci of LBTI (LBT Interferometer), as it is shown in Figure 1, using two deployable dichroics to feed the two SHARK channels. In this way, on the VIS side, the IR light is totally transmitted to LBTI, while on the NIR side, the NIR light will be sent to SHARK-NIR. The dichroics may be positioned just before the entrance window of LBTI, the latter transmitting the IR light to the interferometric focus and reflecting the VIS light to the Pyramid WFS. Such a dichroic, on the VIS channel would pick-up only a certain amount (selectable) of the VIS light, to feed with the rest the WFS, while on the NIR channel would pick up up only the Y, J and H bands, letting all the visible light going through. With this setup, SHARK will provide possible contemporary observations with three instruments at the same time from R to K bands. Such a flexible configuration with several combined binocular observing modes is reflecting the request coming from the principal science cases, for which simultaneous observations in the VIS and NIR domain are required.

SHARK-NIR is a camera for direct imaging coronagraphy and spectroscopy, using the corrected wavefront provided by the LBT Adaptive Secondary Mirror (ASM), operated through one of the existing LBTI AO WFS.

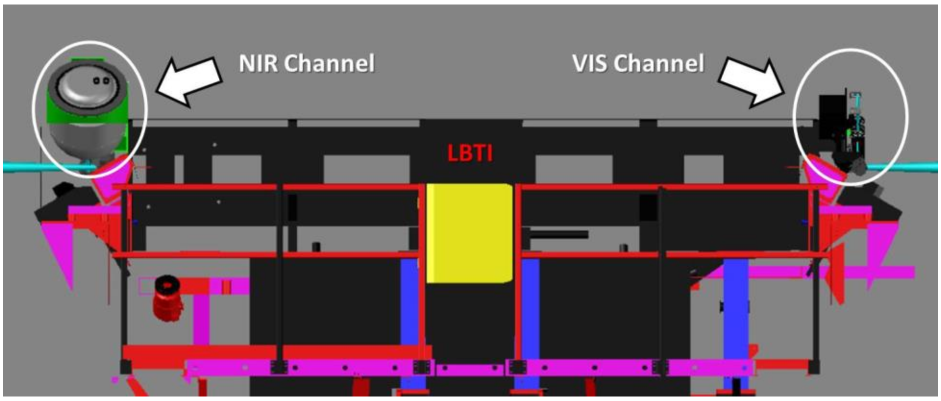

Figure 1: a possible installation of the two SHARK channels at the LBTI entrance foci

The instrument is designed to accomplish an extreme performance, ideally not to decrease the correction provided by the AO system. In fact, all the coronagraphic techniques that may be implemented need a SR as high as possible to provide very good contrast. This requires optics machined to a state of the art technology and polished to nanometric level of roughness, properly aligned and installed on very robust mounts. The whole instrument mechanics has to be very stiff and designed to minimize the effects of flexures.
Additionally, to maintain the performance as good as possible at every observing altitude, it is necessary to implement an atmospheric dispersion corrector (ADC) to compensate for the atmospheric dispersion. Some of the foreseen science cases need to perform the field de-rotation, to accomplish which the whole instrument has to be mounted on a mechanical bearing.
A NIR camera, based on an Teledyne H2RG detector, cooled at about 80°K to minimize the thermal background, will provide a FoV of the order of 18"x18" operating in Y, J and H bands, with a plate scale foreseeing a bit more than two pixels on the diffraction limit PSF at 0.96µm.
A few subsystems have been introduced in the instrument design with the purpose of optimizing the instrument performance.
For the non-common path aberrations (NCPA) minimization, a local DM (ALPAO DM 97-15) has been introduced into the first pupil plane, allowing a local removal of the aberrations. The same DM, used in Tip-Tilt (T-T) fashion, may be used to correct undesired PSF movements during a scientific exposure. The latter correction requires a dedicated T-T sensor (based on the First Light C-RED2 camera), which has been placed after the first pupil plane, into the collimated beam (a beam splitter will pick-up few percent of the light and will send it to the sensor). A Wave Front Computer (WFC, which will be realized by Microgate) will allow the fast T-T correction achieved with the DM, which will at the same time maintain the proper shape for the Non Common Path Aberrations (NCPA) local compensation.

Between the DM and the beam splitter feeding the T-T sensor, a filter wheel positioned at 50mm from the pupil plane carries the apodizing masks. These kinds of masks are normally placed exactly into the pupil plane, which is occupied by the DM in our design. We have carefully evaluated the impact of having the masks slightly displaced with respect to the pupil plane, and it turned out that the effect is basically negligible with the considered coronagraphic techniques if the masks are designed to take this fact into account.

Concerning coronagraphy, a few of techniques will be implemented into the instrument, in a way to fulfill as much as possible the different needs of the different science cases (in terms of contrast and Inner Working Angle - IWA), and the baseline is to provide:

- Gaussian Lyot, which requires a gaussian stop into the 1st focal plane and a pupil stop on the 2nd pupil plane
- Shaped Pupil, which requires an apodizing mask into the 1st pupil plane and an occulting mask into the 1st focal plane
- Four Quadrant, which requires a "knife edge" like mask into the 1st focal plane and a pupil stop on the 2nd pupil plane

The opto-mechanical design of SHARK-NIR is shown in Figure 2, where all the main components are highlighted.
.

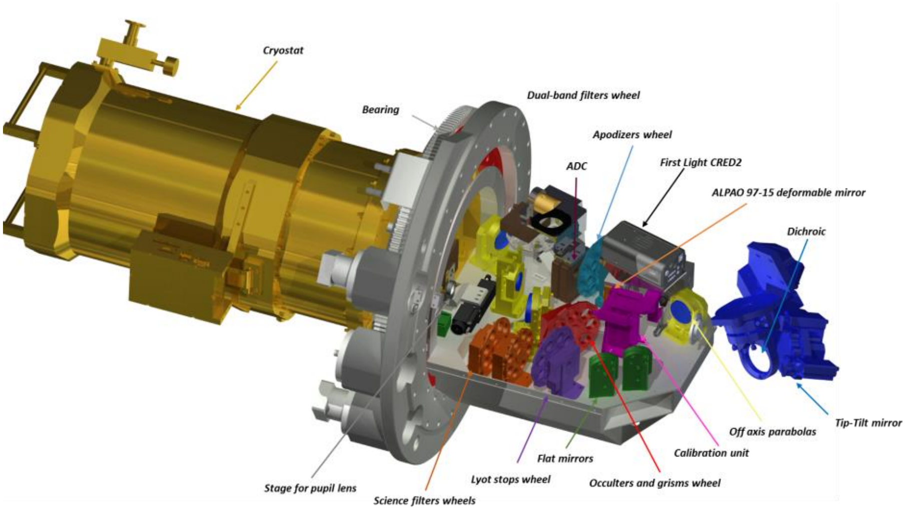

Figure 2: the opto-mechanical concept of the SHARK-NIR optical bench

3. INSTRUMENT STATUS

As already mentioned, SHARK-NIR is in the AIV phase. All the main components/sub-systems have been individually tested, and in the following we briefly report about these activities.

3.1 Calibration Unit Lamps

The Calibration unit lamps have been tested in terms of the typical warm up time and stability, acquiring measurements every second with a NIR photodiode. The average of several test is giving as a result a flux variation <2% after 5 minutes, which is going down to <0.5% of flux variation after 1 hour (see Figure 3).

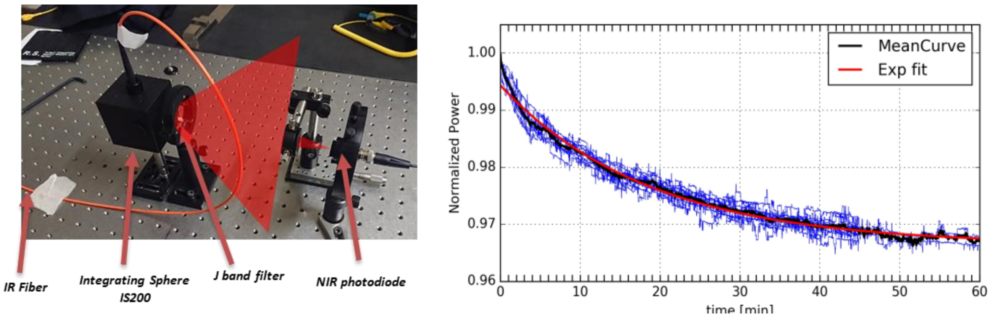

Figure 3: the calibration unit lamp test setup (left) and the test result (right)

3.2 Integrating Sphere Uniformity

We have measured the luminosity distribution provided by the integrating sphere, using a detector whose response was previously characterized. Despite its small dimensions (2 inches), the integrating sphere provides luminous uniformity of ~96% (see Figure 4).

Formattato: Tipo di carattere: Non Corsivo

Formattato: Normale, Allineato a sinistra

Formattato: Didascalia, Allineato a centro, Rientro: Sinistro: 0 cm

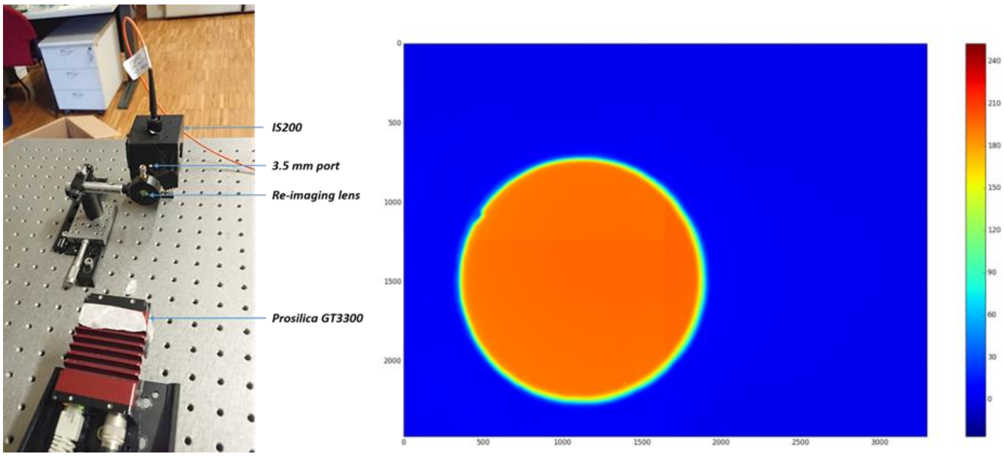

Figure 4: the Integrating Sphere test setup (left) and test result (right) in term of exit port uniformity

3.3 Off-Axis parabolas

We have measured the off-axis distance of the 4 Off-Axis parabolic mirrors, using a Coordinate Measuring Machine (CMM), with an accuracy of ~ 30 µm (see test setup in Figure 5). They are all within specification.

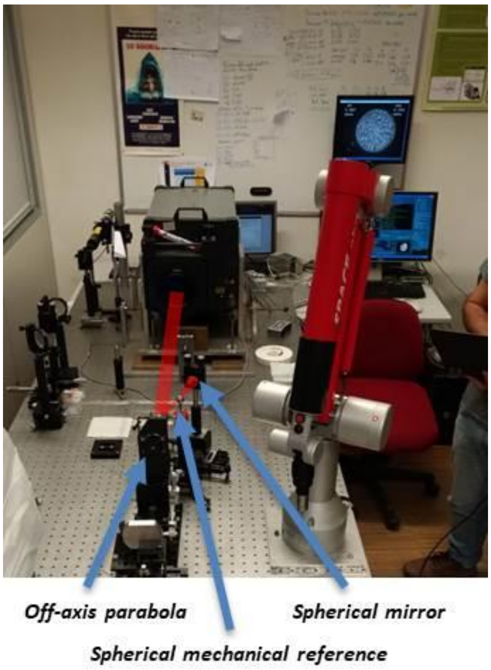

Figure 5: Off-Axis distance measurement test setup

The four off-axis parabolas have been also characterized both at the company premises and in our laboratory in terms of optical quality, and the two measurements are in very good agreement (in Figure 6 we show the characterization performed in our lab).

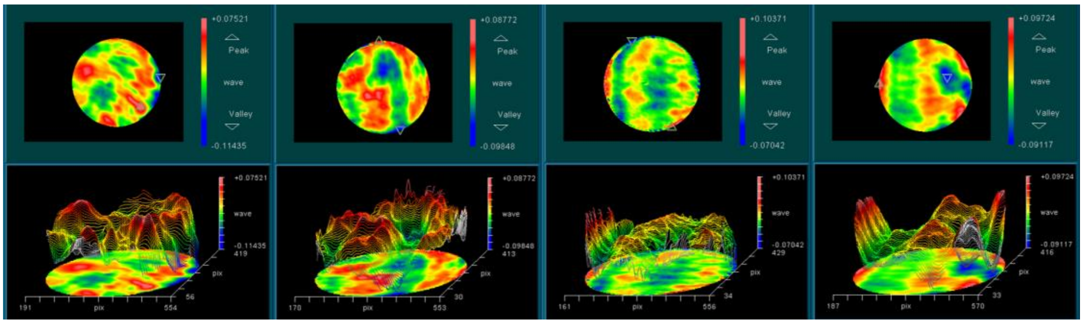

Figure 6: the interferograms characterizing the 4 off-axis parabolas optical quality; this is the reflected wavefront error, which is twice the parabolas surface

3.4 Optical Quality of the Science Filters

We have measured the transmitted optical quality of all the scientific filters of SHARK-NIR. After the analysis, some of them have been rejected and they are being re-manufactured. In Figure 7 there is an example of the interferometric measurements performed.

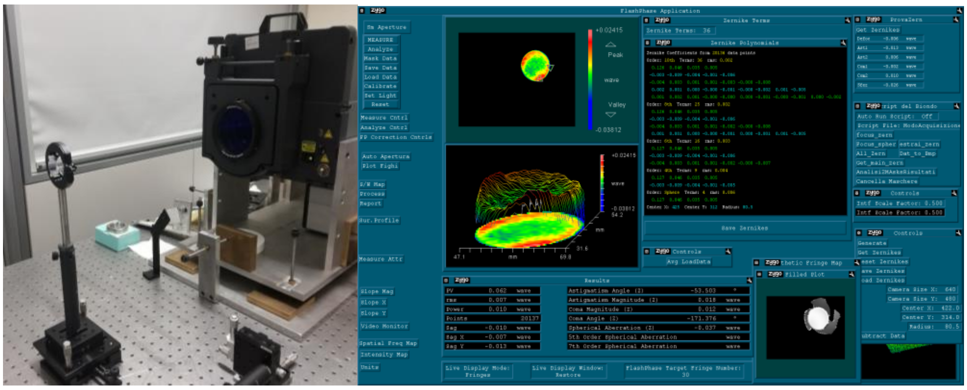

Figure 7: on the left panel, the filters measurement test setup, while on the right an example of the optical quality measured using the interferometer

3.5 Motorized stages test

On each motorized stage which is going to be installed on the bench, we did performs a number of test, which are summarized in the following:

- Functional test to check the general behavior of the stage
- Limit switch positioning accuracy, when applicable
- Minimum incremental step
- Position repeatability

In Figure 8 there is a scheme which summarizes all the motorized stages of the SHARK-NIR bench, while in Figure 9 there is a summary of all the test performed on the various stages.

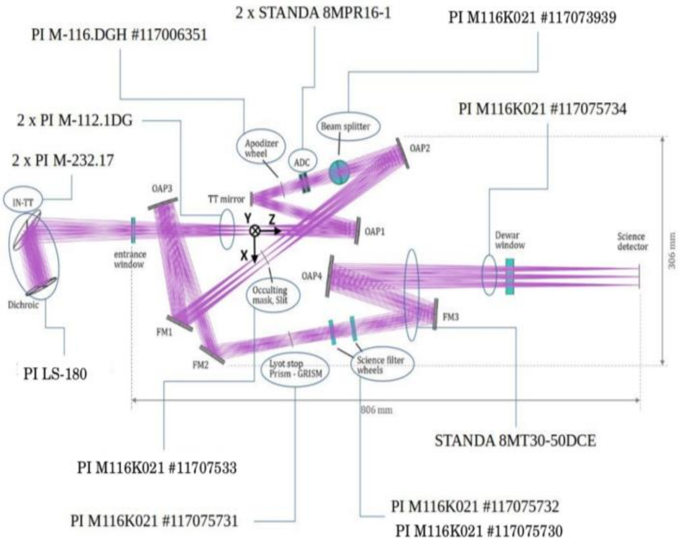

Figure 8: the motorized stages of the SHARK-NIR bench

Stage and scope — The results from the tests conducted on the Standa and PI stages by using the final software. Minimum incremental step and position repeatability values are reported and compared to the SDA requirement	*Test results*		*SDA requirement*
	Minimum incremental step	*Position repeatability*	
PI M-112.1DG #117071802 Calibration mirror deployer	0.5µm	Pos. rep. 2.4µm rms Tilt 3.2arcsec Decenter 4.6µm	/
PI M-112.1DG #117050805 Fiber deployer	0.5µm	Pos. rep. 2.7µm rms Tilt 7.1arcsec Decenter 8µm	Pos. rep. to be simulated Min. inc. step < 1 µm
PI M-116.DGH #117073939 Wavefront sensor arm ND filter wheel	5arcsec	Pos. rep. 7.2arcsec	/
PI M-116.DGH #117006351 Apodizer wheel	5arcsec	Pos. rep. 5.3arcsec	Pos. rep. < 6arcsec
PI M116K021 #117075733 Coronagraphic masks and slits wheel	5arcsec	Pos. rep. 4.1arcsec	Min. inc. step < 9.5arcsec Pos. rep. < 8arcsec
PI M116K021 #117075731 Lyot stops, grism and Wollaston prism wheel	5arcsec	Pos. rep. 4.5arcsec	/
PI M116K021 #117075732 1st science filter wheel	5arcsec	Pos. rep. 6.4arcsec	/
PI M116K021 #117075730 2nd science filter wheel	5arcsec	Pos. rep. 5.8arcsec	/
PI M116K021 #117075734 Dual band filters wheel	5arcsec	Pos. rep. 4.3arcsec	/
PI M-232.17 #117073935 Tip-Tilt entrance folding mirror adjustments X	To be tested in the cleaning room		min. inc. step 1arcsec
PI M-232.17 #117049586 Tip-Tilt entrance folding mirror adjustments Y	To be tested in the cleaning room		min. inc. step 1arcsec
PI LS-180 #6240500148 Deployable arm for input beam selector	To be tested in the cleaning room		/
PI M-403.2DG #118051931 Integrating sphere filter deployer	5 µm	Pos. rep. 4.6 µm rms Tilt 9.7arcsec Decenter 10.8µm	/
Standa 8MPR16-1 #137366 2nd prism	> 0.01°	Pos. rep. 0.1°	Position accuracy <1.5°
Standa 8MPR16-1 #137367 1st prism	> 0.01°	Pos. rep. 0.02°	Position accuracy <1.5°
Standa 8MT30-50DCE Pupil lens deployer	1µm	Pos. rep. 4.6µm rms Tilt 6arcsec Decenter 8.9µm	Position accuracy <48µm

Figure 9: a summary of the test performed on the motorized axis

3.6 Coronagraphic masks test

We tested all the coronagraphic masks received till now, which are the shape-pupil masks and the four quadrant masks.

Shaped Pupil masks test

Concerning the Shape-Pupil, 3 masks are foreseen to be implemented, characterized by different parameters, such as the Inner Working Angle (IWA) and the Outer Working Angle (OWA) and the discovery space. In Figure 10 we recall the 3 masks geometry.

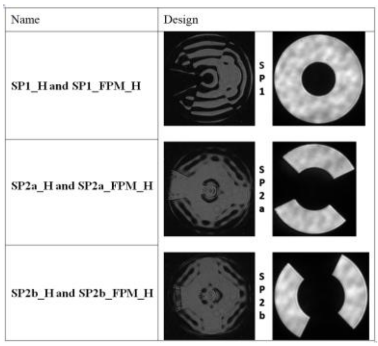

Figure 10: the geometry of the 3 Shaped Pupil masks foreseen to be implemented in SHARK-NIR (left images), and the correspondent discovery space (right images)

An optical bench (see Figure 11) has been prepared on purpose both to check the masks alignment procedure and to test their performance, in term of IWA/OWA and raw contrast.

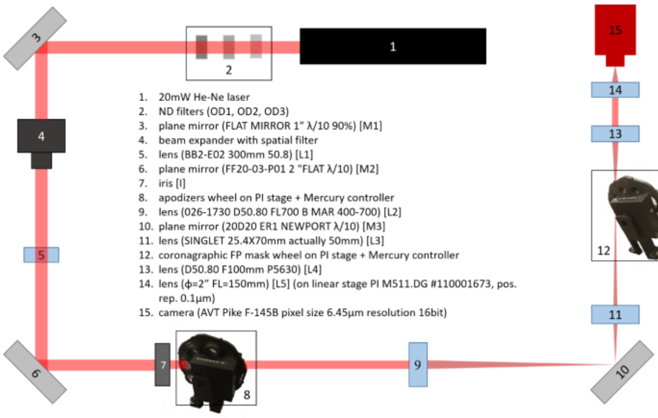

Figure 11: bench setup scheme for the coronagraphic test bench.

The apodizing masks have been of course inserted in the dedicated wheel such that they are aligned with the LBT pupil orientation, and test concerning the foreseen alignment procedure have been carried on, showing that the masks can be aligned within the required accuracy.

In Table 1 we report instead the measured Inner and Outer working angles, which are in very good agreements (within a few microns) with the requested ones.

Coronagraphic mask technique	**IWA [µm]**		**OWA [µm]**	
	theoretical	measured	theoretical	measured
SP1_FPM_H	196	198	528	521
SP2a_FPM_H	262	266	528	521
SP2b_FPM_H	247	250	528	521

Table 1: the IWA and OWA test result on the 3 Shaped Pupil masks

We have also measured the raw contrast of the 3 shaped pupil masks, and compared them with the expected ones. Figure 12 shows such a comparison, and it is quite evident that the measured raw contrasts are in very good agreements with the expected ones in the region of interest, which is between the IWA and the OWA.

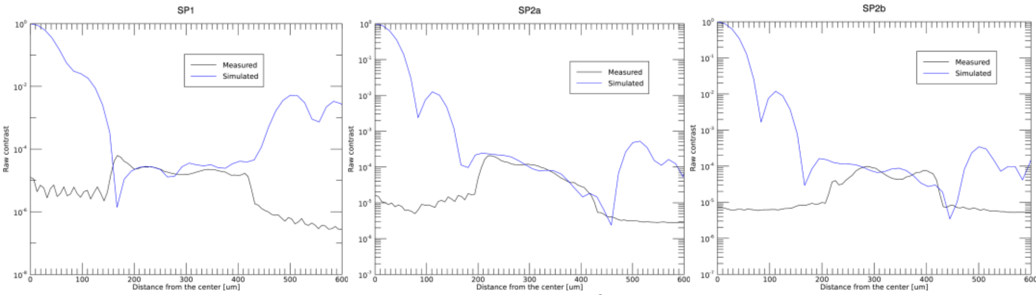

Figure 12: the measured raw contrast for the 3 shaped pupil masks

Four Quadrant mask test

The four quadrant mask realized for SHARK-NIR have been designed by Observatoire de Paris - LESIA, optimized at the wavelength of 1.6µm, in order to provide a rejection of more than a factor 500 in monochromatic light. The PSF peak intensity, with and without the coronagraph, is a function of the wavelength; the phase mask is optimized to work at 1.6µm but, in our case, we have a local minimum also at a wavelength around 550nm (see Figure 13), in a way that we can test this mask in the visible spectrum, which is for several reasons much easier.

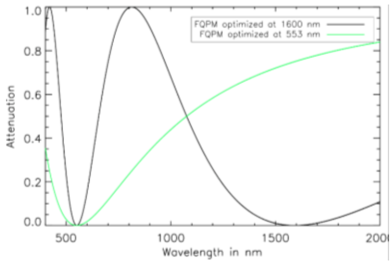

Figure 13: the attenuation of the four quadrant mask vs wavelength

Also in this case, we did set-up a coronagraphic bench to perform the test, which is shown in Figure 14 left side. On the same figure we also show the real images of the pupil and focal planes with the FPQM.

In Figure 15 we report the remarkable result of the test, from which it looks clear that the achievable contrast is of the order of 10^{-5} averaged over the full FoV of the mask, and it becomes even better in selected areas of the discovery space.

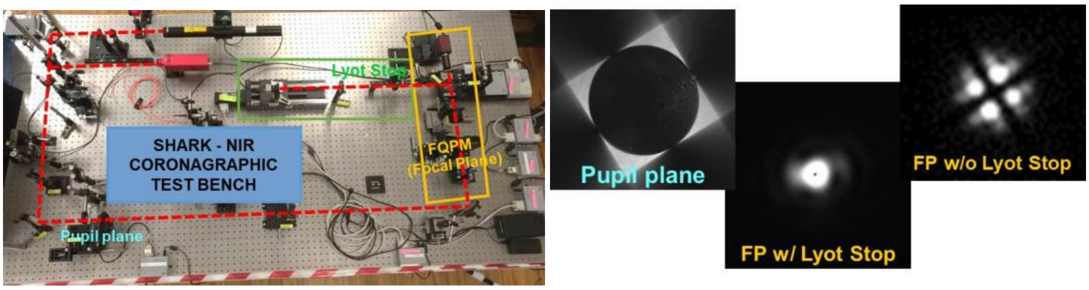

Figure 14: on the left, the opto-mechanical setup used to test the FPQM; on the right, the real images of the mask generated in the intermediate pupil and focal planes

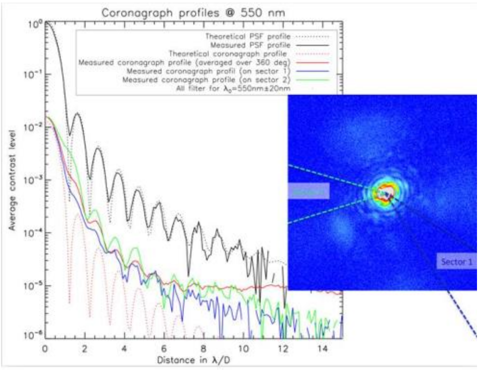

Figure 15: The result of the FPQM test, in red the coronagraphic profile averaged over the whole discovery space

3.7 Fast Tip-Tilt loop, NCPA correction and DM characterization

SHARK-NIR includes an Adaptive Optics channel composed by a 97-actuators Deformable Mirror, a NIR-camera as wavefront sensor, and a Real Time Computer to coordinate the loop. Its main tasks are the correction of the Non Common Path Aberrations and of the residual Tip-Tilt of the LBT-AO.

We characterize the AO-channel in Padova laboratory in order to understand the capability to close the Tip Tilt loop at different R-magnitudes (R=8,9,10) and different frame rates (500,1000 Hz) when a Tip Tilt history is introduced in the optical path (sending the disturbance directly to the DM) with different amplitude (15, 10, 5, 0 mas). In Table 2 we show which are the rms spread of the centroid positions when we close the loop starting from a combination of input parameters.

R magnitude	Input time history / Frame Rate [Hz]	15 mas	10 mas	5 mas	No input time-history
Mag 8	500	5.7	4.6	2.1	0.9
	1000	3.2	1.5	1.2	0.4
Mag 9	500	5.9	4.1	1.3	1.6
	1000	3.3	3.2	2.9	2.4
Mag 10	500	6.8	4.3	2.8	1.4
	1000	---	---	---	---

Table 2: performance of the tip-tilt loop in term of rms spread of the centroid positio

Then we explore which is the efficiency of the system to maintain a NCPA correction during a TT loop. To achieve this, we applied to the DM a shape the total rms of which is the one estimated through the instrument error budget (corresponding to about 100nm), generated with the proper spectrum, also estimated in the instrument error budget. In this case we use a SH-WF in order to track the stability of 30 Zernike's modes during a TT loop: the rms of the distribution of the single aberration mode does not exceed 4 nm, and there is no significant difference among the values in open loop (with time history applied) and closed loop. The overall error on the wavefront in term of rms is given by the quadrature sum of each Zernike term rms contribution, and gives a value of the order of 8nm in the worst case. We can thus conclude that the shape assumed by the DM to correct for the NCPA is maintained down to <10nm of shape rms during the fast tip-tilt loop operations.

We also test the hardware components of the AO-channel, in particular we performed an intense characterization of the DM: we define an influence matrix and create a modal base defined on the full pupil and on a smaller one. Moreover, we highlight these particular features:

1) There is no memory effect;
2) There is no impact of magnetic field induced by the filter wheel.
3) The thermal effects are difficult to disentangle from creep effect (see next item) when working outside of a cleanroom. We measure about 8 nm rms Power on the flat shape from outside (about 22°C) to inside the cleanroom (20°C)

4) We measure a creep effect whose drift is about 13% of the given command, for each poked mode.

3.8 Software

SHARK-NIR control Software (SHINS) design and architecture are described in [19], from which Figure 16 is extracted. The design is inspired to VLT instrument control software, a central component controlling peripheral components each responsible for a subsystem, while operations are executed by means of so called *template* scripts.

Currently SHINS is under development and test; almost the completeness of the motorized functions has been implemented, as well as the interface with the scientific camera control software, the telescope control system and the software component responsible for sequencing the observation blocks. The implementation of the three sub-components controlling each the calibration functions, the real-time tip/tilt subsystem and the tracking functions is ongoing, with the latter being the most critical, requiring the synchronization of the devices with the motion of the telescope during observation. All of these information are reported in Figure 16.

During this phase SHINS is supporting the integration phase in clean room, allowing a more thorough test of the implemented functionalities.

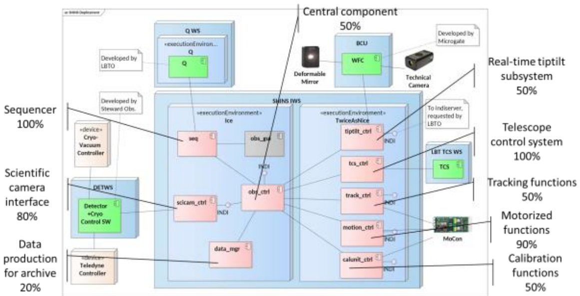

Figure 16: the control software architecture and the level of completeness of each sub-component.

CONCLUSIONS

SHARK-NIR is in the AIV phase, and the current schedule is foreseen that the Preliminary Acceptance Europe will be held in May 2020. The instrument shall than be shipped to LBT in June 2020, and installed at the telescope during next summer shut-down.

Once obtained the LBT board green-light, the SHARK-NIR commissioning will start, and hopefully the instrument will be ready for on-sky observation in mid-2021.

REFERENCES

[1] Farinato, J.; Pedichini, F.; Pinna, E.; Baciotti, F.; Baffa, C.; Baruffolo, A.; Bergomi, M.; Bruno, P.; Cappellaro, E.; Carbonaro, L.; Carlotti, A.; Centrone, M.; Close, L.; Codona, J.; Desidera, S.; Dima, M.; Esposito, S.; Fantinel, D.; Farisato, G.; Fontana, A.; Gaessler, W.; Giallongo, E.; Gratton, R.; Greggio, D.; Guerra, J. C.; Guyon, O.; Hinz, P.; Leone, F.; Lisi, F.; Magrin, D.; Marafatto, L.; Munari, M.; Pagano, I.; Puglisi, A.; Ragazzoni, R.; Salasnich, B.; Sani, E.; Scuderi, S.; Stangalini, M.; Testa, V.; Verinaud, C.; Viotto, V.; "SHARK (System for coronagraphy with High order Adaptive optics from R to K band): a proposal for the LBT 2nd generation instrumentation", SPIE Proc. 9147, id. 91477J 10 pp. (2014).

[2] Hill, J. M. and Salinari, P., "Large Binocular Telescope project," Proc. SPIE, 4004, 36–46 (2000).

[3] Stangalini, M.; Pedichini, F.; Centrone, Mauro; Esposito, S.; Farinato, J.; Giallongo, E.; Quirós-Pacheco, F.; Pinna, E.; "The solar system at 10 parsec: exploiting the ExAO of LBT in the visual wavelengths", SPIE Proc. 9147, id. 91478F 7 pp. (2014).

[4] Farinato, J., Baffa, C., Baruffolo, A., Bergomi, M., Carbonaro, L., Carlotti, A., Centrone, M., Codona, J., Dima, M., Esposito, S., Fantinel, D., Farisato, G., Gaessler, W., Giallongo, E., Greggio, D., Hink, P., Lisi, F., Magrin, D., Marafatto, L., Pedichini, F., Pinna, E., Puglisi, A., Ragazzoni, R., Salasnich, B., Stangalini, M., Verinaud, C. and Viotto, V., "The NIR arm of SHARK (System for coronagraphy with High order Adaptive optics from R to K band)", International Journal of Astrobiology, 14(3), 365-373 (2015)

[5] Esposito, S., Riccardi, A., Pinna, E., Puglisi, A. T., Quirós-Pacheco, F., Arcidiacono, C., Xompero, M., Briguglio, R., Busoni, L., Fini, L., Argomedo, J., Gherardi, A., Agapito, G., Brusa, G., Miller, D. L., Guerra Ramon, J. C., Boutsia, K. and Stefanini, P. "Natural guide star adaptive optics systems at LBT: FLAO commissioning and science operations status", Proc. SPIE, 8447, 84470U (2012)

[6] Ragazzoni, R., "Pupil plane wavefront sensing with an oscillating prism," Journal of Modern Optics 43, 289 (1996).

[7] Riccardi, A.; Xompero, M.; Briguglio, R.; Quirós-Pacheco, F.; Busoni, L.; Fini, L.; Puglisi, A.; Esposito, S.; Arcidiacono, C.; Pinna, E.; Ranfagni, P.; Salinari, P.; Brusa, G.; Demers, R.; Biasi, R.; Gallieni, D.; "The adaptive secondary mirror for the Large Binocular Telescope: optical acceptance test and preliminary on-sky commissioning results", SPIE 7736, 79 (2010)

[8] Hinz, P.M., Angel, J.R.P., McCarthy, D.W., Hoffman, W.F., and Peng, C.Y., "The large binocular telescope interferometer," in Proc. SPIE, 4838, 108 (2003).

[9] Pinna, E., Pedichini, F., Farinato, J., Esposito, S., Centrone, M., Puglisi, A., Carbonaro, L., Agapito, G., Riccardi, A., Xompero, M., Hinz, P., Montoya, M., and Bailey, V., "XAO at LBT: current performances in the visible and upcoming upgrade," Proc. of AO4ELT4 conference.

[10] Ragazzoni, R.; Farinato, J.; "Sensitivity of a pyramidic Wave Front sensor in closed loop Adaptive Optics", A&A, 350, L23 (1999)

[11] Vérinaud, C.; Le Louarn, M.; Korkiakoski, V.; Carbillet, M.; "Adaptive optics for high-contrast imaging: pyramid sensor versus spatially filtered Shack-Hartmann sensor", MNRAS, 357, L26 (2005)

[12] Esposito, S.; Riccardi, A.; "Pyramid Wavefront Sensor behavior in partial correction Adaptive Optic systems", A&A, 369, L9 (2001)

[13] Costa, Joana B.; Feldt, Markus; Wagner, Karl; Bizenberger, Peter; Hippler, Stefan; Baumeister, Harald; Stumpf, Micaela; Ragazzoni, Roberto; Esposito, Simone; Henning, Thomas; "Status report of PYRAMIR: a near-infrared pyramid wavefront sensor for ALFA", SPIE Proc. 5490, 1189 (2004)

[14] Ghedina, Adriano; Cecconi, Massimo; Ragazzoni, Roberto; Farinato, Jacopo; Baruffolo, Andrea; Crimi, Giuseppe; Diolaiti, Emiliano; Esposito, Simone; Fini, Luca; Ghigo, Mauro; Marchetti, Enrico; Niero, Tiziano; Puglisi, Alfio; "On Sky Test of the Pyramid Wavefront Sensor", SPIE Proc. 4839, 869 (2003)

[15] Beuzit, J.-L.; Boccaletti, A.; Feldt, M.; Dohlen, K.; Mouillet, D.; Puget, P.; Wildi, F.; Abe, L.; Antichi, J.; Baruffolo, A.; Baudoz, P.; Carbillet, M.; Charton, J.; Claudi, R.; Desidera, S.; Downing, M.; Fabron, C.; Feautrier, P.; Fedrigo, E.; Fusco, T.; Gach, J.-L.; Giro, E.; Gratton, R.; Henning, T.; Hubin, N.; Joos, F.; Kasper, M.; Lagrange, A.-M.; Langlois, M.; Lenzen, R.; Moutou, C.; Pavlov, A.; Petit, C.; Pragt, J.; Rabou, P.; Rigal, F.; Rochat, S.; Roelfsema, R.; Rousset, G.; Saisse, M.; Schmid, H.-M.; Stadler, E.; Thalmann, C.; Turatto, M.; Udry, S.; Vakili, F.; Vigan, A.; Waters, R.; "Direct Detection of Giant Extrasolar Planets with SPHERE on the VLT", ASP Proc. 430, 231 (2010)

[16] Macintosh, B. A., Graham, J. R., Palmer, D. W., Doyon, R., Dunn, J., Gavel, D. T., Larkin, J., Oppenheimer, B., Saddlemyer, L., Sivaramakrishnan, A., Wallace, J. K., Bauman, B., Erickson, D. A., Marois, C., Poyneer, L. A., and Soummer, R., "The Gemini Planet Imager: from science to design to construction," Proc. SPIE 7015, 31 (2008).

[17] Close, L. M.; Males, J. R.; Kopon, D. A.; Gasho, V.; Follette, K. B.; Hinz, P.; Morzinski, K.; Uomoto, A.; Hare, T.; Riccardi, A.; Esposito, S.; Puglisi, A.; Pinna, E.; Busoni, L.; Arcidiacono, C.; Xompero, M.; Briguglio, R.; Quiros-Pacheco, F.; Argomedo, J., "First closed-loop visible AO test results for the advanced adaptive secondary AO system for the Magellan Telescope: MagAO's performance and status", SPIE Proc. 8447, 0 (2012)

[18] Guyon, O.; Martinache, F.; Clergeon, C.; Russell, R.; Groff, T.; Garrel, V.; "Wavefront control with the Subaru Coronagraphic Extreme Adaptive Optics (SCExAO) system", SPIE Proc. 8149, 894293 (2011)

[19] De Pascale, M; Baruffolo, A; Salasnich B.; Bergomi, M.; Briegel, F.; D'Orazi, V.; Downey, E.C.; Farinato, J.; Hinz, M.H.; Marafatto, L.; Mohr, L.; Viotto, V.; "Design of SHINS: the SHARK-NIR INstrument control Software", SPIE Proc. 7019, 70191Y-1